# *p*H-dependent x-ray absorption spectra of aqueous boron oxides

Andrew M. Duffin,[1,2] Craig P. Schwartz,[1,2] Alice H. England,[1,2] Janel S. Uejio,[1,2] David Prendergast,[3] and Richard J. Saykally[1,2,a)]
[1]*Department of Chemistry, University of California, Berkeley, California 94720, USA*
[2]*Chemical Sciences Division, Lawrence Berkeley National Laboratory, Berkeley, California 94618, USA*
[3]*Molecular Foundry, Lawrence Berkeley National Laboratory, Berkeley, California 94720, USA*

(Received 13 December 2010; accepted 18 March 2011; published online 18 April 2011)

Near edge x-ray absorption fine structure (NEXAFS) spectra at the boron K-edge were measured for aqueous boric acid, borate, and polyborate ions, using liquid microjet technology, and compared with simulated spectra calculated from first principles density functional theory in the excited electron and core hole (XCH) approximation. Thermal motion in both hydrated and isolated molecules was incorporated into the calculations by sampling trajectories from quantum mechanics/molecular mechanics simulations at the experimental temperature. The boron oxide molecules exhibit little spectral change upon hydration, relative to mineral samples. Simulations reveal that water is arranged nearly isotropically around boric acid and sodium borate, but the calculations also indicate that the boron K-edge NEXAFS spectra are insensitive to hydrogen bonding, molecular environment, or salt interactions.
 [doi:10.1063/1.3574838]

## I. INTRODUCTION

In the past decade, considerable effort has been directed to the study of borohydrides as hydrogen storage materials.[1] Hydrolysis of borohydride produces molecular hydrogen and an oxygenated boron compound. In spite of these efforts, the U.S. Department of Energy (DOE) recently gave a "no-go" recommendation for an automotive sodium borohydride system.[2,3] A significant factor contributing to this recommendation is the excess water required for hydration of hydrolysis reaction products—borate [$B(OH)_4$)] in particular. Borate is significantly less soluble than borohydride, further complicated by the formation of polyborate ions, so excess water is required to keep borate in solution. The excess water reduces the wt. % hydrogen storage, one of the main considerations for automotive fuels. In an effort to better understand the hydration of boron oxides, we performed near edge x-ray absorption fine structure (NEXAFS) spectroscopy experiments to probe boric acid, borate, and polyborate ions in solution. We also compare the measured boron spectra with calculated spectra generated using the recently developed excited electron and core hole (XCH) method.[4]

In their own right, borate and boric acid [$B(OH)_3$] are interesting because they comprise an atypical acid/base pair. The change from acid to conjugate base is not a simple deprotonation, but instead involves a reaction with water and a change in boron coordination. In addition, at high concentrations (>0.025 M), boric acid evolves through a series of polyborate anions as a function of *p*H, as evident in Reactions (1)–(4).

$$\overset{\text{boric acid}}{B(OH)_3} + H_2O \leftrightarrows \overset{\text{borate}}{B(OH)_4^-} + H^+, \tag{1}$$

$$\overset{\text{triborate}}{3B(OH)_3} \leftrightarrows B_3O_3(OH)_4^- + H^+ + 2H_2O, \tag{2}$$

$$\overset{\text{tetraborate}}{4B(OH)_3} \leftrightarrows B_4O_5(OH)_4^{2-} + 2H^+ + 3H_2O, \tag{3}$$

$$\overset{\text{pentaborate}}{5B(OH)_3} \leftrightarrows B_5O_6(OH)_4^- + H^+ + 5H_2O. \tag{4}$$

The reactions involved in aqueous boron chemistry have been extensively studied using NMR and electrochemical techniques.[5–13] Figure 1 depicts the speciation of boron compounds in a 0.5 molar boric acid solution as a function of *p*H, as derived from published reaction constants.[5–8] The graph plots the fraction of total boron in each of the four species included in this study (pentaborate ion excluded due to low abundance).

Inspection of aqueous boric acid chemistry clearly shows that the water surrounding boron molecules is vital for the acid/base reaction and the formation of polyborate ions. Boric acid is a trigonal planar molecule with an empty $2p_z$ orbital perpendicular to the molecular plane. The conjugate base, borate, is tetrahedrally coordinated. Water reacting with boric acid must hybridize the empty $2p_z$ orbital. Consequently, aqueous boric acid would be expected to show considerable hydration-dependent effects compared to solid samples.

Moreover, sodium ions have been shown by a variety of techniques to associate with borate anions in aqueous solutions,[14–17] according to Reaction (5),

$$Na^+ + B(OH)_4^- \leftrightarrows NaB(OH)_4. \tag{5}$$

Beyond effects on solubility, sodium–borate association in water is significant because it affects speciation and isotopic fractionation. This information has been used to

a)Author to whom correspondence should be addressed. Electronic mail: saykally@berkeley.edu. Telephone: (510) 642-8269.

 

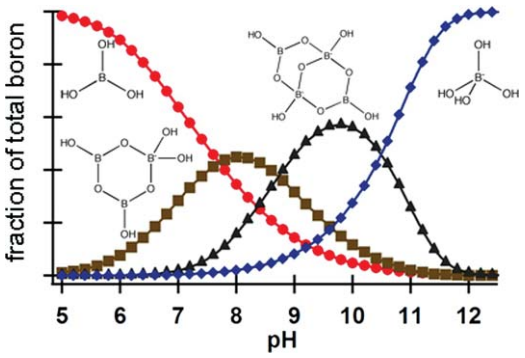


FIG. 1. Boron oxide speciation as a function of *p*H. Calculated for a 0.5 M boric acid solution, the plot shows the fraction of the total boron in each of the species (structure indicated on graph) as a function of *p*H. Circles—boric acid; squares—triborate; triangles—tetraborate; diamonds—borate.

model water–rock interactions and to calculate the *p*H of ancient oceans.[17–20]

X-ray absorption spectroscopy (XAS) spectra of boron-containing minerals, glasses, and gasses have been studied previously.[21–28] The main peaks in mineral and glass boron samples, attributed to trigonal and tetrahedral boron, are sensitive to the ratio of trigonal and tetrahedral boron as well as B–O bond length.[21] The main trigonal boron peak at 194 eV is attributed to the transition of an electron from the B 1s state to the unoccupied B $2p_z$ orbital. A second trigonal boron peak at higher energy (204 eV), above the ionization potential (IP), is attributed to transitions from B 1s to unoccupied B–O $\sigma^*$ orbitals. The main absorption feature in tetrahedral boron samples (197 eV) lies just above the IP and is assigned to the transition of electrons from B 1s to B–O $\sigma^*$ states.[23] These unoccupied molecular orbitals, directly probed by NEXAFS, typically extend well beyond the excited boron atom/molecule.[29] As a result, we expected that NEXAFS of these species be sensitive to changes in local structure and environment, such as solvation. However, in this work, we find that it is not.

In this study, XAS data for solvated boron compounds were collected using the liquid microjet technique. Microjets allow a thin filament of volatile liquid (~30 $\mu$m) to be injected directly into a high vacuum environment, permitting windowless coupling of the jet chamber to a synchrotron beamline. Incident x-ray photons intersect the liquid filament and total electron yield (TEY) x-ray absorption spectra are collected with a biased copper electrode, yielding the absorption spectrum of the bulk liquid.

## II. METHODS

### A. Samples

Boric acid with a stated purity of ~99.5% was obtained from Fisher Chemical and used without further purification. The *p*H of the 0.5 M boric acid solutions was adjusted with either NaOH or KOH and measured with *p*H paper. The water for all solutions had a resistivity of 18 MΩ/cm.

### B. NEXAFS spectroscopy

Boron K-edge total electron yield spectra were obtained on Beamline 8.0.1 of the Advanced Light Source at Lawrence Berkeley National Laboratory. A detailed description of the experimental endstation and data collection has been published elsewhere.[30] Briefly, the undulator at Beamline 8 produces an intense beam ($>10^{11}$ photons/s) of highly resolved ($E/\Delta E > 4000$), tunable photons. The soft x-rays from the beamline are focused to a spot size of ~50 $\mu$m onto a liquid jet ~30 $\mu$m in diameter. The x-rays intersect the liquid just as it emerges from the nozzle, yielding a room-temperature absorption spectrum. A major advantage of using a liquid jet is that the sample is continually refreshed and, consequently, sample damage contamination of the measured signal is minimized. The jet itself is created by using a syringe pump (Teledyne-ISCO) to pressurize liquid behind a small piece of fused silica capillary that acts as the jet nozzle. Another advantage of using a liquid jet is that the endstation, with a few differential pumping sections, can be coupled directly to the beamline, without a flux reducing window.

The pressure in the jet chamber is kept low ($10^{-4}$ Torr) with a turbomolecular pump and by skimming and then cryotrapping the liquid jet. This working pressure is sufficiently low to allow for efficient and sensitive charged particle detection. XAS spectra were collected by incrementing the photon energy (0.2 eV step size) across the boron adsorption edge, 190–215 eV. The total electron yield, in this case providing a bulk measurement, was collected with a biased copper electrode located approximately 1 cm from the jet. The current from the electrode was amplified, converted to a voltage, and then converted to a frequency before being read into the beamline computer.

The TEY signals were normalized to the signal from a gold mesh ($I^o$) ~3 m upbeam from the jet chamber. A background vapor spectrum, collected off jet, was also subtracted from each sample to correct the baseline. Multiple spectra for each sample were averaged and the resulting spectral area normalized for comparison. Photon energy was calibrated by collecting TEY spectra for solid boric acid.

### C. Calculations

X-ray induced core level excitations occur on attosecond time scales and essentially sample molecules in frozen structural configurations, thermodynamically sampled from the accessible vibrational or conformational degrees of freedom. Consequently, the experimental spectra show peaks that are broadened due to the thermally occupied vibrational levels (in addition to zero point motion).[31,32] To accurately simulate the experimental measurements, the spectra from multiple molecular dynamics snapshots, sampling the natural range of vibrational motion, need to be calculated and averaged. To accomplish the vibrational sampling, each molecule is solvated in a periodic box and quantum mechanics/molecular mechanics (QM/MM) simulations are run at 300 K (Langevin thermostat) for 10 ns. QM/MM calculations were run to accurately simulate the motion of the solvated boron molecule

in the absence of easily implemented empirical potentials for boron. The periodic boxes contained between 76 and 141 water molecules depending on the size of the solute. The modified neglect of differential overlap (MNDO) Hamiltonian was used for the QM calculations of the boron species and snapshots were collected every 100 ps.[33] The nonbonding (Lennard-Jones) parameters for boron were taken from Pletnev.[34]

For each of the 100 snapshots generated in the MD simulations, an x-ray absorption spectrum was calculated. The snapshot average was used as the final simulated spectrum. The methods for calculating XAS have been described previously.[4,31] Briefly, density functional theory (DFT) employing a plane wave basis set and periodic boundary conditions was used to calculate spectra. The exchange-correlation energy was estimated within the generalized-gradient approximation with the Perdew–Burke–Ernzerhof exchange-correlation functional.[35] A plane wave basis set was chosen to accurately predict both localized and delocalized states. The final electronic states were calculated using a boron pseudopotential with a core hole (electronic configuration $1s^1 2s^2 2p^2$) and one extra valence electron. These excited electron and core hole calculations explicitly include both the full core hole and the corresponding excited core electron promoted to the lowest energy unoccupied valence state. Self-consistent charge densities and states were calculated using the plane wave self consistent field (PWSCF) code within the QUANTUM ESPRESSO package.[36] The transition amplitude was estimated using the single particle and dipole approximations.[4] Calculations were performed using the Franklin supercomputer at the National Energy Research Scientific Computing Center.

Boron K-edge NEXAFS spectra were calculated for boric acid, borate, triborate, and tetraborate. For the polyborate molecules, spectra were separately calculated for the trigonal and tetrahedral boron species. All spectra were uniformly broadened using a GAUSSIAN convolution of 0.2 eV full width at half maximum. To partially correct bandwidth underestimation within DFT, all calculated spectra were stretched along the energy axis by 10%. The calculated spectra were empirically aligned to experimental absorption onset.

## III. RESULTS AND DISCUSSION

The solid lines in Fig. 2 show boron K-edge NEXAFS spectra of 0.5 M boric acid solutions for a series of *p*H values. Similar to solid and gas samples, solvated boron oxides show three main spectral features. The lowest energy feature at 194 eV corresponds to the transition from a B 1s state to the empty B $2p_z$ orbital of trigonal boron. As the *p*H increases, the percentage of trigonal boron decreases. For that reason, the intensity of the low energy peak decreases with increasing *p*H and is absent at high *p*H. Trigonal boron has a second broad feature centered at 204 eV that corresponds to transitions from B 1s to B–O $\sigma^*$ orbitals. Tetrahedrally coordinated boron oxides have only one broad absorption feature beginning at about 197 eV that matches with a transition from the B 1s to the B–O $\sigma^*$ states. These $\sigma^*$ absorption features have been shown to correlate with bond length, but no attempt at this type of analysis is made herein. As the *p*H increases, and with it the percentage of tetrahedral boron, the intensity of the feature at 197 eV increases. It is interesting to compare the solvated boron spectra with spectra of similar gas phase boron molecules.[26–28] Although the energies of the peaks are different due to an oxygen rather than a halide bond, the spectra are surprisingly similar.

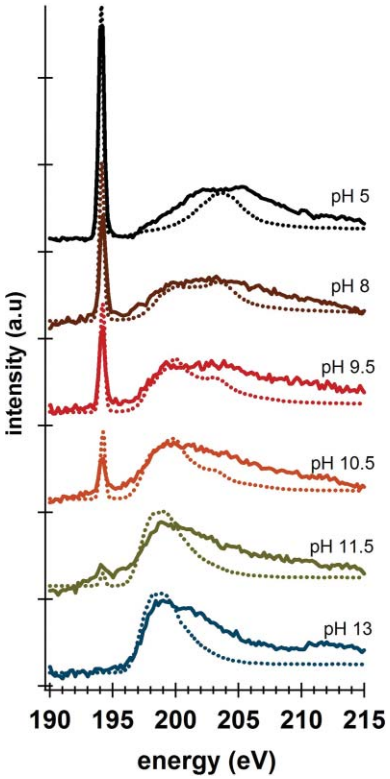


FIG. 2. Experimental and theoretical B K-edge NEXAFS spectra showing the transition from trigonal to tetrahedrally coordinated boron with *p*H. The spectra are of 0.5 M boric acid solutions at a series of *p*H values, increasing *p*H top to bottom as indicated on figure. For each *p*H value the solid line is the experimental spectrum and the dotted line is the associated spectrum from calculations.

The dotted lines in Fig. 2 are the calculated spectra. The final calculated spectrum at a given *p*H is a linear combination of the spectra from individual species combined according to the ratios in Fig. 1. In general, the calculated spectra are in excellent agreement with the experimental spectra; although, the high energy sides of the calculations do not reproduce the measured intensity. The energy axis has been stretched by 10% to compensate for expected underestimation of the unoccupied density of states bandwidth within DFT. However, we have no guarantee that systematic DFT errors are uniform with energy. In practice, we may expect larger upward shifts in energy for more localized states, as recently observed for water by Chen *et al.*[37] In addition, multiple scattering resonances contribute to the experimental intensity, whereas they are absent in the present calculations. Although the calculations do not fully reproduce the experimental intensity on the high energy side, they account for all the salient features of the spectra.

In addition, the high energy feature for the boric acid sample, *p*H 5, is broader than evident in the corresponding

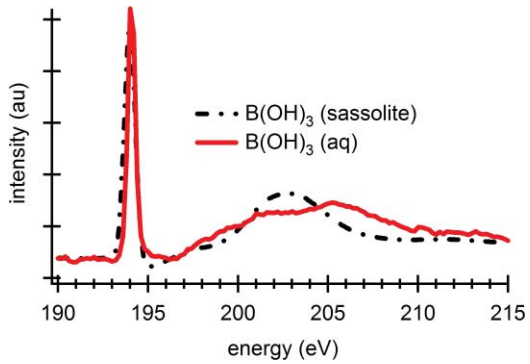


FIG. 3. Boron K-edge NEXAFS spectra for aqueous (solid line) and solid (dashed line) boric acid. Solid boric acid, sassolite, data provided by Fleet and Liu (Ref. 21).

calculations. Given the propensity for boron oxides to form polyborate ions, it is reasonable to expect considerable interaction of boric acid monomers. For concentrated boric acid/borate solutions, Ishihara *et al.*[9] attributed a coalesced NMR signal to a symmetrical dimer transition state between boric acid and borate. If present in sufficient concentrations, dimers similar to those proposed by Ishihara *et al.*[9] may give detectable concentrations of tetrahedrally bonded boron and result in the broad high energy feature observed in our experiments. The QM/MM simulations used for the calculations did not account for short range solute–solute interactions. Analysis of the broad high energy boric acid peak with calculations simulating multiple solute molecules could reveal clues to polyborate ion formation and would constitute an interesting future project.

Figure 3 compares the TEY NEXAFS spectra of hydrated boric acid with mineral boric acid (sassolite) (Ref. 21) (data provided by Fleet). The low energy peak at 194 eV is nearly identical in the two samples. Clearly, water does not significantly affect the $2p_z$ unoccupied orbital. The acid-base transition from three coordinate (boric acid) to four coordinate (borate) boron requires water to hybridize with this $2p_z$ orbital. Consequently, it would be expected that solvation should include water interacting with the B $2p_z$ orbital. Water interacting with this nonbonding orbital would shift it in energy relative to the same orbital in the solid. No such shift in energy is observed for the low energy feature in hydrated versus solid boric acid.

Furthermore, the trigonal boron peak at 194 eV does not show any shifts (within the experimental resolution) associated with *p*H/incorporation into polyborate ions. Not only is the unoccupied $2p_z$ orbital unaffected by solvating water, it is also insensitive to changes in the extended bonding environment. The energy of the transition to the $2p_z$ orbital does not change based on whether the trigonal boron is monomeric or part of a polyborate ion. The results are similar for the high energy feature (204 eV). The calculations reveal minor changes in the shape of this high energy trigonal boron feature (204 eV) between monomer and polyborate borons, but if present, these subtle changes cannot currently be determined experimentally. Moreover, spectra calculated by summing only the appropriate spectral contribution from monomers (as opposed to monomers and polyborate ions) are nearly identical to the calculated spectra in Fig. 2. Clearly, extended bonding environment, i.e., monomer versus polyborate ion, has no observable spectral influence for solvated boron oxide molecules.

Figure 3 also shows that the solid boric acid sample has a much narrower higher energy feature (204 eV) compared to that of solvated boric acid. Again, solute–solute interactions in the liquid may be responsible for the broad high energy feature in the experimental boric acid spectrum. Interestingly, the spectrum of the solid sample is very similar to the spectrum calculated for solvated boric acid.

Based on the general environmental insensitivity evident in the solvated boron oxides, it is not surprising that borate spectra exhibit no cation-dependent changes. NEXAFS spectra for sodium borate and potassium borate solutions, not shown, were indistinguishable within the noise of the measurement. Similarly, increasing the concentration of sodium cations in solution had no effect on the spectrum. The MD simulations of sodium borate indicated that sodium nearly always remains in contact with the borate. The Na–boron radial distribution function was strongly peaked at 2.6 Å and no sodium was found farther than 3.3 Å away from the boron. In spite of such a close Na–borate association, calculations also confirm that sodium has no spectral influence. Figure 4 shows the calculated borate spectrum compared to a similar spectrum calculated from simulations run without sodium. Within the error of the calculations, they are identical. Going one step further, Fig. 4 also shows calculated spectra for boric acid and borate with all the water molecules removed. Again, within the error of the calculations, water

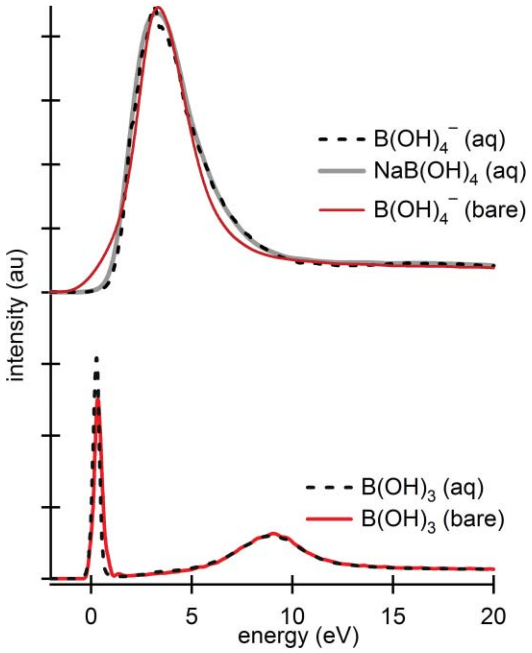


FIG. 4. Calculations of borate NEXAFS spectra in the presence and absence of sodium cations and/or water. The upper section shows calculations for aqueous borate, aqueous sodium borate, and bare borate. There are no significant spectral changes between the three. Similarly, there are no significant spectral changes between aqueous boric acid and bare boric acid shown in the lower section.

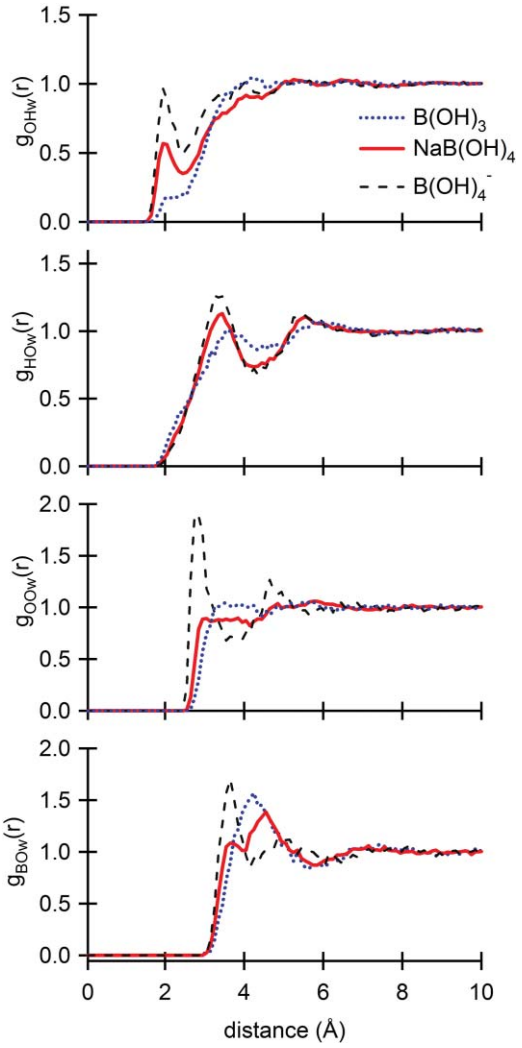


FIG. 5. Radial distribution functions calculated from MD simulations. From top to bottom: O to H–water, H to O–water, O to O–water, and B to O–water. In each plot the dotted blue line is boric acid, the solid red line is sodium borate, and the dashed black line is borate (without sodium). As evidenced by the change in peak height at 2 Å (top plot), the cation disrupts the donation of hydrogen bonds to the borate oxygens. For boric acid there are also few donor hydrogen bonds because the lone pairs on the oxygens contribute to the pi system in the trigonal planar molecule. H to O–water bonds (upper middle plot) are less affected by the cation, but the freely rotating H's on borate lead to greater variability in hydrogen bonds donated to water. Interactions between H's and O's within the molecule also diminish the oxides ability to donate a hydrogen bond to water. The disruption of hydrogen bonds by the cation is even more evident in the O to O–water RDF (lower middle). The B to O–water RDF (bottom) gives a relatively broad peak indicative of weak hydrogen bonding to water.

induces no significant spectral changes to the boron oxide spectra.

The presence of hydroxide moieties on boric acid and borate would lead one to believe that these oxides would strongly hydrogen bonded with the surrounding water; however, this is not evident in the molecular dynamics simulations. Figure 5 displays various radial distribution functions (RDF) for boric acid, borate, and sodium borate calculated from the simulations. The radial distribution functions (and spatial distribution functions not shown here) give evidence that water is arranged nearly isotropically around boric acid and sodium borate. For boric acid, the lone pairs on the oxygens donate to the empty $2p_z$ orbital on the boron, making the lowest energy conformation trigonal planar. Consequently, there are fewer waters that donate a hydrogen bond to the boric acid oxygens as evidenced by the low intensity shelf at 2 Å in the O–$H_{water}$ RDF. Similarly, the trigonal conformation allows the boric acid hydrogens to partially donate to intramolecular oxygens. This limits the number of hydrogen bonds that boric acid donates. These data are consistent with the temperature dependant solubility of boric acid, since increased temperature would disrupt the planar molecular configuration and lead to increased interaction with water. Consequently, it may be possible to observe temperature dependent solvent effects for boric acid.

The data are similar for the sodium borate system; however, in this case the lack of strong hydrogen bonds is due to cation association rather than conformation. The borate (without sodium) O–$H_{water}$, O–$O_{water}$, and B–$O_{water}$ RDFs all show relatively sharp peaks at distances that indicate strong hydrogen bonds with water. However, in the presence of the sodium cation, these peaks are reduced, disappear, and/or broaden considerably. That is, sodium cations displace the waters around the borate ion and prevent water from donating hydrogen bonds to the borate. As in the case with boric acid, the ability of the borate hydrogens to associate with intramolecular borate oxygens leads to a relatively broad H–$O_{water}$ peak, which, at 3.4 Å, is too long to represent strong hydrogen bonds. The simulations indicate that boric acid and sodium borate do not strongly associate with water, however, the calculations also show that the boron K-edge spectra are insensitive to hydrogen bonding even if present. The spectra for borate and sodium borate in Fig. 4 are nearly identical even though borate shows evidence for strong hydrogen bonding to water and sodium borate does not.

Water seems to have no spectral impact on these boron oxides because the states involved in the absorption are insensitive to the environment. To further investigate this environmental insensitivity, we inspect a few states contributing to the main XAS features. Figure 6 shows the calculated spectra and associated states (10% isosurface), both hydrated and bare, for an individual boric acid snapshot, with energies defined relative to the absorption onset and provided without dilation. The high energy feature (~8 eV above the absorption onset on the unshifted/unstretched axis of Fig. 6) comprises of transitions to a myriad of states, but only one is shown for clarity. As expected, the empty $2p_z$ state (LUMO), is responsible for the sharp peak at the absorption onset. This state is nearly identical in the hydrated and bare molecules (leftmost states in upper and lower portions of Fig. 6). In spite of the fact that water must change this state to form the conjugate base, there is no evidence that this state interacts with water upon hydration. Also as expected, the higher energy feature (8 eV in Fig. 6) is clearly $\sigma^*$ in character. Even though there is some mixing with water states, for the most part these $\sigma^*$ states are unaffected by hydration. Similar conclusions can be drawn by inspecting states from bare and hydrated borate ions.

XAS data of solvated boron oxides are surprisingly similar to data from boron containing solids. In corroboration,

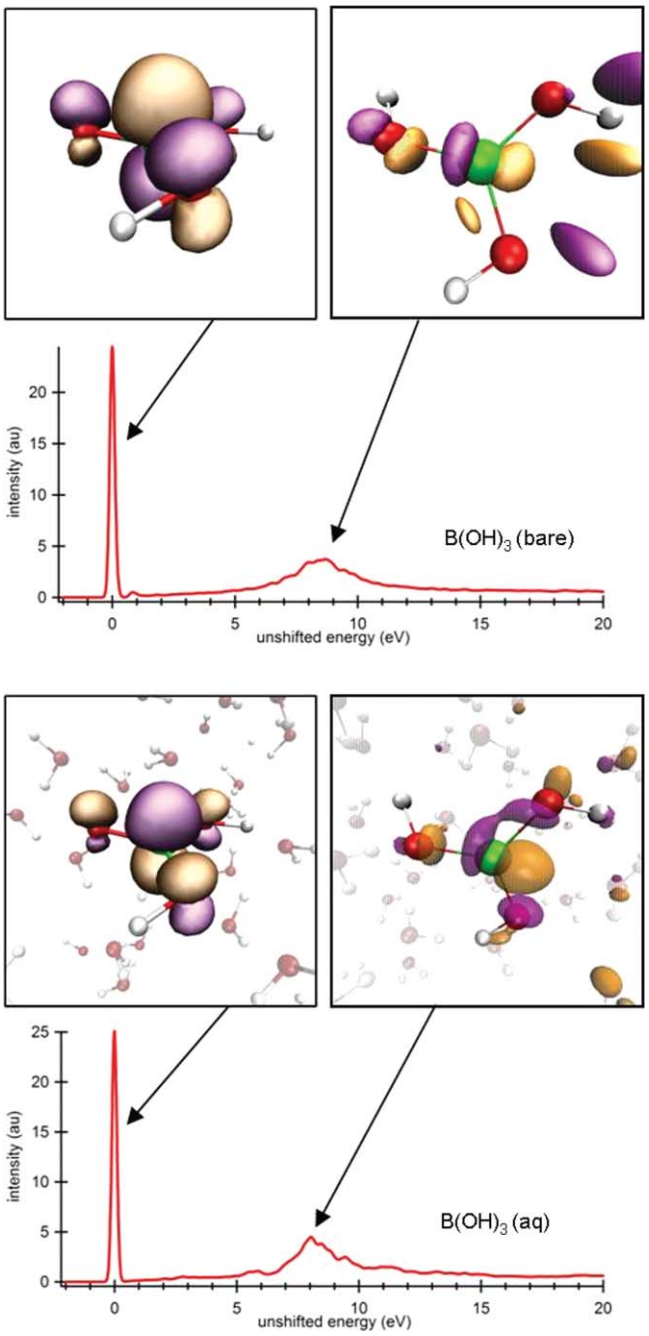


FIG. 6. Single snapshot spectra and associated states (10% isosurface) for bare boric acid (upper) and fully hydrated boric acid (lower). The LUMO state, the empty $2p_z$ orbital, responsible for the sharp low energy transition at 0 eV (energy adjusted to LUMO energy and unstretched) is nearly identical for the bare and hydrated cases. The LUMO states are the boxed images on the left. Water does not interact significantly with this empty $2p_z$ orbital. The $\sigma^*$ states to the right are some of the many responsible for the high energy feature (~8 eV). The local $\sigma^*$ character is preserved upon hydration and there is minimal mixing with water. The fine structure in the spectrum is averaged out in an ensemble of snapshots.

molecular dynamics simulations with electronic structure calculations indicate that boron oxides do not strongly interact with water and that water is arranged nearly isotropically around boric acid and sodium borate. These observations invite speculation concerning the mechanism of the boron oxide acid/base reaction as well as polyborate ion formation.

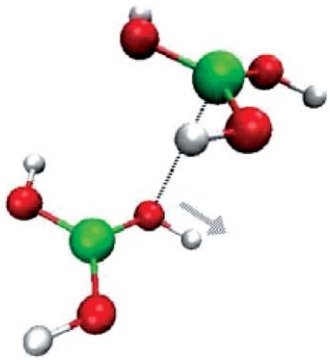

SCHEME 1.

A boric acid–borate dimer has already been proposed for the exchange between tetrahedral borate and trigonal boric acid.[9] Initial formation of the dimer may proceed through hydrophobic collapse of boric acid monomers followed by simple deprotonation. Scheme 1 shows a possible mechanism in which a boron from a boric acid coordinates with an oxygen from an adjacent boric acid. The overcoordinated oxygen is then more likely to donate a proton to the surrounding water. Similarly, polyborate ion formation likely proceeds via hydrophobic collapse of a third (and then fourth) boric acid monomer followed by elimination of water. Further information may be gained by measuring and comparing boric acid NEXAFS spectra taken at low and high concentrations. Low concentration data would presumably sample monomers and the spectra may be different from high concentration spectra. Simulations run with multiple solutes would also be useful for interpreting the experimental spectra.

## IV. CONCLUSIONS

Since water plays such an integral role in the acid–base and polyborate ion formation reactions of aqueous boron oxides, it would be expected that these molecules be strongly hydrated. Moreover, the presence of hydroxide moieties on these boron compounds implies that there should be strong hydrogen bonds to water. However, the boron K-edge NEXAFS spectra of aqueous boron oxides proved to be insensitive to hydrogen bonding. Corresponding calculations reveal that the states responsible for the observed NEXAFS features are mainly localized on the boron containing molecule. That is, there is very little state mixing between the boron oxide and the surrounding water and the calculations confirm the insensitivity of the measurements to intermolecular interactions. However, the molecular dynamics simulations reveal that water is arranged nearly isotropically around boron oxides. The lack of strong water–solute interactions may contribute to the tendency of boron oxides to form polyborate ions in solution.

## ACKNOWLEDGMENTS

This work was supported by the Director, Office of Basic Energy Sciences, Office of Science, U.S. Department of Energy under Contract No. DE-AC02-05CH11231, through the LBNL Chemical Sciences Division and the Molecular

Foundry. Computational resources were provided by NERSC, a DOE Advanced Scientific Computing Research User Facility.

[1]U. B. Demirci, O. Akdim, J. Andrieux, J. Hannauer, R. Chamoun, and P. Miele, Fuel Cells **10**, 335 (2010).
[2]See http://www.hydrogen.energy.gov/pdfs/42220.pdf for "Go/No-Go Recommendation for Hydrolysis of Sodium Borohydride for On-Board Vehicular Hydrogen Storage."
[3]U. B. Demirci, O. Akdim, and P. Miele, Int. J. Hydrogen Energy **34**, 2638 (2009).
[4]D. Prendergast and G. Galli, Phys. Rev. Lett. **96**, 215502 (2006).
[5]C. G. Salentine, Inorg. Chem. **22**, 3920 (1983).
[6]L. Maya, Inorg. Chem. **15**, 2179 (1976).
[7]J. E. Spessard, J. Inorg. Nucl. Chem. **32**, 2607 (1970).
[8]N. Ingri, Acta Chem. Scand. **17**, 573 (1963).
[9]K. Ishihara, A. Nagasawa, K. Umemoto, H. Ito, and K. Saito, Inorg. Chem. **33**, 3811 (1994).
[10]R. E. Mesmer, C. F. Baes, and F. H. Sweeton, Inorg. Chem. **11**, 537 (1972).
[11]T. Hirao, M. Kotaka, H. Kakihana, and M. Maeda, J. Inorg. Nucl. Chem. **41**, 1217 (1979).
[12]R. K. Momii and N. H. Nachtrie, Inorg. Chem. **6**, 1189 (1967).
[13]N. Ingri, Acta Chem. Scand. **17**, 581 (1963).
[14]E. J. Reardon, Chem. Geol. **18**, 309 (1976).
[15]H. Corti, R. Crovetto, and R. Fernandezprini, J. Solution Chem. **9**, 617 (1980).
[16]L. M. Rowe, L. B. Tran, and G. Atkinson, J. Solution Chem. **18**, 675 (1989).
[17]G. S. Pokrovski, J. Schott, and A. S. Sergeyev, Chem. Geol. **124**, 253 (1995).
[18]A. Sanyal, N. G. Hemming, G. N. Hanson, and W. S. Broecker, Nature (London) **373**, 234 (1995).
[19]N. G. Hemming and G. N. Hanson, Geochim. Cosmochim. Acta **56**, 537 (1992).
[20]M. Pagani, D. Lemarchand, A. Spivack, and J. Gaillardet, Geochim. Cosmochim. Acta **69**, 953 (2005).
[21]M. E. Fleet and X. Liu, Phys. Chem. Miner. **28**, 421 (2001).
[22]R. Carboni, G. Pacchioni, M. Fanciulli, A. Giglia, N. Mahne, M. Pedio, S. Nannarone, and F. Boscherini, Appl. Phys. Lett. **83**, 4312 (2003).
[23]M. E. Fleet and S. Muthupari, Am. Mineral. **85**, 1009 (2000).
[24]M. E. Fleet and S. Muthupari, J. Non-Cryst. Solids **255**, 233 (1999).
[25]M. Kasrai, M. E. Fleet, S. Muthupari, D. Li, and G. M. Bancroft, Phys. Chem. Miner. **25**, 268 (1998).
[26]E. Ishiguro, S. Iwata, Y. Suzuki, A. Mikuni, and T. Sasaki, J. Phys. B **15**, 1841 (1982).
[27]N. Kosugi, T. Yokoyama, and H. Kuroda, Chem. Phys. **104**, 449 (1986).
[28]W. H. E. Schwarz, L. Mensching, K. H. Hallmeier, and R. Szargan, Chem. Phys. **82**, 57 (1983).
[29]J. Stöhr, *NEXAFS Spectroscopy* (Springer-Verlag, Berlin, 1992).
[30]K. R. Wilson, B. S. Rude, J. Smith, C. Cappa, D. T. Co, R. D. Schaller, M. Larsson, T. Catalano, and R. J. Saykally, Rev. Sci. Instrum. **75**, 725 (2004).
[31]J. S. Uejio, C. P. Schwartz, R. J. Saykally, and D. Prendergast, Chem. Phys. Lett. **467**, 195 (2008).
[32]C. P. Schwartz, J. S. Uejio, R. J. Saykally, and D. Prendergast, J. Chem. Phys. **130**, 184109 (2009).
[33]D. A. Case, T. E. Cheatham, T. Darden, H. Gohlke, R. Luo, K. M. Merz, A. Onufriev, C. Simmerling, B. Wang, and R. J. Woods, J. Comput. Chem. **26**, 1668 (2005).
[34]D. S. Otkidach and I. V. Pletnev, J. Mol. Struct.:THEOCHEM **536**, 65 (2001).
[35]J. P. Perdew, K. Burke, and M. Ernzerhof, Phys. Rev. Lett. **77**, 3865 (1996).
[36]P. Giannozzi, S. Baroni, N. Bonini, M. Calandra, R. Car, C. Cavazzoni, D. Ceresoli, G. L. Chiarotti, M. Cococcioni, I. Dabo, A. Dal Corso, S. de Gironcoli, S. Fabris, G. Fratesi, R. Gebauer, U. Gerstmann, C. Gougoussis, A. Kokalj, M. Lazzeri, L. Martin-Samos, N. Marzari, F. Mauri, R. Mazzarello, S. Paolini, A. Pasquarello, L. Paulatto, C. Sbraccia, S. Scandolo, G. Sclauzero, A. P. Seitsonen, A. Smogunov, P. Umari, and R. M. Wentzcovitch, J. Phys. Condens. Matter **21**, 395505 (2009).
[37]W. Chen, X. F. Wu, and R. Car, Phys. Rev. Lett. **105**, 017802 (2010).